Structure and Dynamics of the Lantibiotic Mutacin 1140[†]

Leif Smith,[‡,§] Cherian Zachariah,[||] Ramanan Thirumoorthy,[⊥,#] Jim Rocca,[∇] Jan Novák,[@] J. D. Hillman,[+,§] and Arthur S. Edison*,[‡,||,∇]

University of Florida Interdisciplinary Graduate Program in Neuroscience, Gainesville, Florida 32611, Department of Biochemistry and Molecular Biology, University of Florida, Box 100245, Gainesville, Florida 32610-0245, Department of Chemistry, University of Florida, Buckman Drive, Gainesville, Florida 32611, Advanced Magnetic Resonance Imaging and Spectroscopy Facility in the McKnight Brain Institute of the University of Florida and National High Magnetic Field Laboratory, Gainesville, Florida 32611, Department of Microbiology, University of Alabama at Birmingham, Birmingham, Alabama 35294, and Department of Oral Biology, University of Florida, Gainesville, Florida 32611

Received March 27, 2003; Revised Manuscript Received June 13, 2003

ABSTRACT: Mutacin 1140 is a member of a family of ribosomally synthesized peptide bacteriocins called lantibiotics (lanthionine-containing antibiotics) and is produced by the Gram-positive bacterium *Streptococcus mutans*. Mutacin 1140 has been shown to be effective against a broad array of Gram-positive bacteria. Chromatography and mass spectroscopy data suggested that mutacin 1140 forms a small compact structure. Nuclear magnetic resonance (NMR) data and restrained molecular dynamics simulations showed that mutacin 1140 interconverts between multiple structures. Calculations of scalar (J) coupling constants showed the best agreement with experimental values when the entire population-weighted ensemble of structures was used, providing independent support for the ensemble. Representative structures from each major group in the ensemble had a common feature in which they are all kinked around the hinge region forming a horseshoe-like shape, and the regions of flexibility of the molecule were limited and well-defined. The structures determined in this study provide a starting point for modeling the mutacin 1140-membrane interactions and pore formation.

Mutacin is a posttranslationally modified lantibiotic peptide produced by *Streptococcus mutans* JH1140 (*1*). In earlier work, the covalent structure of mutacin 1140 was characterized (*2*). The covalent structure of mutacin 1140 (Figure 1) contains four thioether rings and is similar to other type A lantibiotics such as gallidermin (*3*−*5*) and epidermin (*6*). Thioether rings contain a single sulfur atom and link two amino acids through their β-carbons. This work laid the foundation for the 3-D structure work presented in this paper.

Very few 3-D structures of type A lantibiotics have been determined. Currently, structures have been solved for nisin in water, nisin in SDS and dodecylphosphocholine micelles, and gallidermin in trifluoroethanol/water (95:5) (*5*, *7*−*10*). In each of these structures, NOEs were observed only within the lanthionine rings, and no long-range NOEs were observed between the rings or the other regions of the primary sequence (*5*, *7*−*11*). NMR[1] and molecular dynamic simulations showed that the global structure of nisin is an extended peptide with a flexible, obtuse angle between the N- and the C-termini and that gallidermin forms a fairly rigid structure with an overall screw-like shape (*5*, *7*−*10*). Nisin was shown to be a very flexible peptide, which was different from the well-defined folding pattern exhibited by gallidermin. However, the lanthionine ring structures in both nisin and gallidermin were fairly rigid and well-defined.

Lantibiotics function by forming transmembrane pores, but an isolated lantibiotic monomer is too small to form a pore. Therefore, the mode of bactericidal activity of type A lantibiotics is believed to involve monomer aggregation followed by the disruption of the cytoplasmic membrane causing the efflux of ions, ATP, and other essential cellular components. Most type A lantibiotics have a net positive charge, while Gram-positive bacteria normally have a high content of anionic lipids. The electrostatic interactions

---

[†] This work was supported in part by Grants DEO4529, DE12327, and T32 DE7200 from the National Institute of Dental and Craniofacial Research and by 5P41RR016105-02 from the NCRR. A.S.E. was supported by an NSF CAREER award.

* To whom correspondence should be addressed. E-mail: art@mbi.ufl.edu. Fax: (352) 392-3422. Phone: (352) 392-4535.

[‡] University of Florida Interdisciplinary Graduate Program in Neuroscience.

[§] Present address: Oragenics, Inc., 12085 Research Dr., Alachua, FL 32615.

[||] University of Florida, Department of Biochemistry and Molecular Biology.

[⊥] University of Florida, Department of Chemistry.

[#] Present address: Department of Biological Sciences, State University of New York at Buffalo, Buffalo, NY 14260.

[∇] McKnight Brain Institute of the University of Florida and National High Magnetic Field Laboratory.

[@] University of Alabama at Birmingham.

[+] Department of Oral Biology, University of Florida.

[1] Abbreviations: Lan, lanthionine; MeLan, β-methyl-lanthionine; Dha, 2,3-didehydroalanine; Dhb, 2,3-didehydrobutyrine; Ala$_S$, alanyl moiety of lanthionine and β-methyl-lanthionine; Abu$_S$, β-methyl-alanyl moiety of β-methyl-lanthionine; Abu, 2-aminobutyric acid; Av, amino vinyl group; S-EC, thioethyl cysteine; β-M-S-EC, β-methylthioethyl cysteine; NMR, nuclear magnetic resonance; NOESY, nuclear Overhauser enhancement spectroscopy; TOCSY, total correlation spectroscopy.

10.1021/bi034490u CCC: $25.00

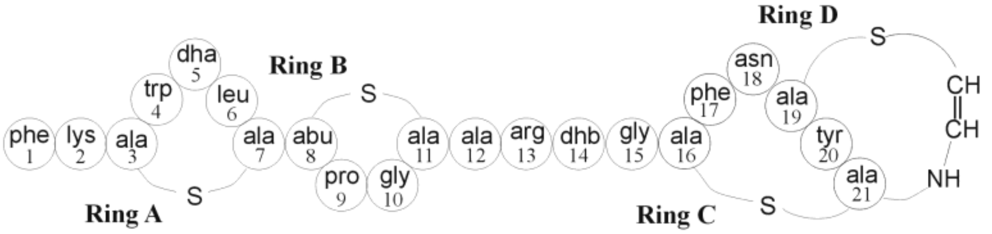

FIGURE 1: Covalent structure of the lantibiotic mutacin 1140.

between the lantibiotic and the bacterial membrane are believed to be required for initial binding. Experiments with nisin have demonstrated that the sensitivity of the host bacterium is due to the relative amount of anionic phospholipids in the membrane (*12*, *13*). In addition, cell−bacteriocin interactions are enhanced by the presence of docking molecules such as lipid II for nisin (*14*, *15*).

The bactericidal activity of mutacin 1140 includes a broad array of Gram-positive bacteria, many of which are responsible for diseases. Importantly, genetically stable resistant variants of sensitive strains have not yet been found, suggesting that the structure and chemistry of mutacin 1140 may provide important information for the development of new antibiotics as well as a better understanding of its antimicrobial activity. Thus, for several reasons, it is important to obtain a comprehensive understanding of the 3-D structure of mutacin 1140. The 3-D structure of mutacin 1140 was determined in acetonitrile/water (80:20). The global structure of nisin in aqueous solution is essentially the same when bound to micelles (*7*). Thus, the structure determined in acetonitrile/water (80:20) is a reasonable starting point to predict the orientation of the membrane-bound molecule. Like nisin and gallidermin, the thioether ring structures of mutacin 1140 were rigid and well-defined, and like nisin the regions not spanned by thioether linkages were quite flexible (*5*, *7*, *10*). These flexible regions may be important for bactericidal activity by allowing the lantibiotic to orient properly in the membrane (*13*, *16*). This motif of two domains fixed by lanthionine rings joined by a flexible hinge may be a common feature of type A lantibiotics. However, unlike previous lantibiotic structures, we identified several long-range NOEs outside of thioether rings that define a more compact structure than previously reported. The structure determined in this study is in good agreement with the biochemical properties and allows initial modeling of mutacin 1140/membrane interactions.

EXPERIMENTAL PROCEDURES

All chemicals were purchased from Sigma and were the highest grade, unless otherwise stated. Mutacin 1140 was produced and purified as previously described (*1*).

Size-Exclusion Chromatography. Mutacin 1140 (1 mL of partially purified preparation) was fractionated in 8 M urea (to prevent aggregation) using a calibrated FPLC column (Superdex 75 [10 mm internal diameter, 30 cm long]; Amersham Pharmacia Biotech, Piscataway, NJ). To determine where the biologically active mutacin peptide eluted, 1-mL fractions were collected, and aliquots (25 μL) were assayed for activity by spotting samples of fractions on Todd−Hewitt agar with a lawn of the indicator strain BHT-2 (*1*). The relative molecular size of mutacin 1140 was calculated based on the elution times of bovine serum albumin, 66 kDa; trypsin inhibitor, 21.5 kDa; cytochrome *c*, 12.4 kDa; and a polypeptide tryptic fragment, 2.5 kDa.

Mass Spectrometry. Mutacin 1140 was analyzed by electrospray ionization mass spectrometry (ESI-MS) on a PE Sciex API III biomolecular mass analyzer as described before (*1*). Tandem mass spectrometry (MS/MS) was performed by selecting the parent ion having a particular m/z with the first quadrupole and allowing it to move into the second quadrupole, where it collided with argon atoms and fragmented. The fragments produced were analyzed with the third quadrupole (*2*).

Mercaptoethanol Derivatization of the Mutacin 1140. Mutacin 1140 was chemically modified with β-mercaptoethanol (MeSH) at neutral pH to selectively label only existing dehydrated residues. The sample (12 μL, ∼15 μg) was incubated in 0.1 M ammonium acetate buffer pH 7 with MeSH (3 μL) at 50 °C for 1 h. Samples were then analyzed by ESI-MS and MS/MS.

Tryptic Digest. Mutacin 1140 (about 10 μg) was incubated for 2 h with sequencing-grade trypsin (Sigma) in 0.1 M ammonium acetate buffer pH 7, and the sample was then analyzed by ESI-MS and MS/MS.

NMR Spectroscopy. The NMR sample preparation and the NMR spectroscopy experiments TOCSY acquired at 60 ms mixing time (*17*) and NOESY acquired at 200, 400, and 450 ms (*18*) were collected as described by Smith and co-workers (*2*).

Protons that are buried in the molecule or involved in intramolecular hydrogen bonding exchange more slowly than protons exposed to the solvent. Amide proton/deuterium exchange was measured by dissolving lyophilized protonated mutacin 1140 samples in 80% acetonitrile-d_3 (Cambridge Isotopes) and 20% ^2H_2O (Cambridge Isotopes) yielding a final concentration of ∼2 mM with a volume of 700 μL. 1-D ^1H NMR experiments were collected at 27 °C on a Bruker Avance spectrometer operating at 500 MHz at the Advanced Magnetic Resonance and Imaging Spectroscopy (AMRIS) Facility in the McKnight Brain Institute of the University of Florida. The spectral sweep width was 7507.5 Hz (15 ppm) and was collected with 64K data points. ^1H chemical shifts were referenced to acetonitrile (1.93 ppm). The 1-D spectra were collected at 3−4 min intervals for 1 h.

Some chemical shifts of mutacin 1140 were found to be extremely sensitive to the acetonitrile/water ratio. To characterize these changes, 1-D ^1H NMR experiments were collected at 20 °C on a 600 MHz spectrometer using ∼2 mM samples in 70−90% acetonitrile-d_3 (Cambridge Isotopes) and 10−30% water with a total volume of 700 μL. The spectral sweep widths were 8012.8 Hz (13.35 ppm), and the data were collected with 32K data points. ^{1}H chemical shifts were referenced to acetonitrile (1.93 ppm).

When possible, experimental scalar coupling constants, $^3J^{\mathrm{exp}}_{\mathrm{HNH\alpha}}$, were measured directly from the 1-D spectra in 80% acetonitrile-d_3 (Cambridge Isotopes) and 20% water. When overlap prevented accurate measurements, the couplings were obtained from the 2-D NOESY experiment. A comparison between identical couplings measured with the two types of spectra showed less than 6% difference. Calculated scalar coupling constants, $^3J^{\mathrm{calc}}_{\mathrm{HNH\alpha}}$ (ϕ), were determined for each structure using the computed ϕ angles and the Karplus equation $^3J^{\mathrm{calc}}_{\mathrm{HNH\alpha}}(\phi) = A \cos^2 \theta + B \cos \theta + C$, where $A = 6.4$, $B = -1.54$, $C = 1.25$, and $\theta = |\Phi - 60|$ and $\theta = |\Phi + 60|$ for L-amino acids and D-amino acids, respectively (*19*, *20*). The population-weighted average coupling, $^3J^{\mathrm{av}}_{\mathrm{HNH\alpha}}(\phi)$, for each ϕ angle was calculated using $^3J^{\mathrm{av}}_{\mathrm{HNH\alpha}}(\phi) = \sum_{i=1}^{N_{\mathrm{family}}} c_i\, {}^3J^{\mathrm{calc}}_{\mathrm{HNH\alpha}}(\phi)_i$, where c_i is the population of family i determined from restrained molecular dynamics simulations, $^3J^{\mathrm{calc}}_{\mathrm{HNH\alpha}}(\phi)_i$ is the calculated coupling for family i, and N_{family} is the number of total number of families. Finally, we define a quality factor $Q = \sum_{i=1}^{N_{\mathrm{res}}} |{}^3J^{\mathrm{exp}}_{\mathrm{HNH\alpha}} - {}^3J^{\mathrm{av(calc)}}_{\mathrm{HNH\alpha}}|$, which is the summation over all residues (i) in mutacin 1140. The comparison was made to either the population-weighted average or individual calculated structures.

Computer-Assisted Molecular Modeling (CAMM). NOE cross-peak intensities were measured in NMRView (*21*). Distances were calibrated using the relationship $r_{ab}{}^6 = r_{\mathrm{cal}}{}^6(V_{\mathrm{cal}}/V_{ab})$, where r_{ab} is the distance between atoms a and b, V_{ab} is the NOESY a to b cross-peak volume, r_{cal} is a known distance, and V_{cal} is the corresponding volume of the NOESY calibration cross-peak. The distance used for calibrations was the Tyr^{20} H$^{\delta}$ and H$^{\epsilon}$ aromatic protons (2.46 Å). The NMR NOE data were used as pseudo-potentials in restrained molecular dynamic simulations. Only the interresidue NOE cross-peaks were used as distance restraints in calculations. One Å was added to and subtracted from the calculated distances for upper-bound restraints to pseudo-atoms, and 0.5 Å was added and subtracted to calculated distances for restraints between distinct atoms to define the flat bottom potential energy well. The energy wells were defined using an upper and lower force constant of 1 kcal/mol/Å^2.

All conformational modeling was performed using InsightII software (Accerlys, San Diego, CA). The molecular dynamic simulations were run in a vacuum at 500K with a dielectric constant of 4.0 using the cvff force field with cross-terms, Morse potentials, and 30 Å cutoff distances. The peptide was constructed using the builder function in InsightII. Serine and threonine residues were modified to form 2,3-didehydroalanine (Dha) and 2,3-didehydrobutyrine (Dhb) residues, respectively. These residues form D-isomers when they react with the thiol group of a cysteine residue during the formation of Lan and MeLan residues (*4*, *22*, *23*). Therefore, the 2,3-didehydroalanine and 2,3-didehydrobutyrine residues involved in Lan and MeLan residues formation were hydrogenated and converted to D-amino acids before thioether linkages were formed. The C-terminal cysteine was decarboxylated and converted into *S*-amino vinyl-D-cysteine. Initially, the linear peptide was minimized, and then unrestrained molecular dynamics were run for 10 ps. After this, only the distance restraints of $i + 2$ or greater were added. The molecular dynamic simulations were stopped periodically when the $i + 2$ or greater distance restraints were satisfied among the residues that make up each thioether ring. Ring A was formed first followed by ring B and then intertwined rings C and D. Once the thioether rings were formed, the $i + 1$ distance restraints were added to the $i + 2$ or greater distance restraints, and the molecular dynamic simulation was run for 5 ns at 500K with a dielectric constant of 4.0 using cvff force field with cross terms and Morse potentials. Following this, push away restraints, which consisted of all the NH to NH, Hα to Hα, and NH to Hα that had no visible NOE in the NOESY spectrum that are separated by i+ 3 or more were added to prevent spurious contacts between protons that gave no NOE signal. The energy wells for the push away restraints were defined using a lower force constant of 1 kcal/mol/Å^2 to prevent these protons from coming no closer than 5 Å. Molecular dynamic simulations were run for another 20 ns with all the restraints. History files from the dynamics were written every 10 ps. Two-hundred structures from the history file starting at 1 ns and spaced every 100 ps were energy minimized with all the NMR restraints using 2000 steps of steepest decent followed by conjugate gradients and Newton−Raphson until the root-mean-square (RMS) gradient of the energy of 0.01 kcal/mol/Å was reached. The 200 energy minimized structures were checked for NMR restraint violations using PROCHECK-NMR software (*24*). This software measured the average distances between the restrained nuclei from all 200 energy minimized conformations. Lower- and upper-bound limits were determined by adding and subtracting 1.0 Å to the calculated NOE-derived distances; no violations were said to have occurred if these average distances were between these limits. A total of four restraint violations, none greater than 0.2 Å, were found.

The energy minimized structures were grouped into families using the XCluster program (*25*). The conformations were clustered using the dihedral angles of the backbone atoms and grouped into families of related structures. Families were classified as groups of structures with at least 2% of the total population. A representative structure was determined by XCluster from each family. Using InsightII, the overall RMS deviations and backbone RMS deviations were calculated by superpositioning each representative structure or structural elements of each representative structure determined from each family of structures to the representative structure of the largest family of structures.

RESULTS

Mutacin 1140 Has a Compact Structure. According to ultrafiltration experiments, mutacin 1140 was believed to have a molecular mass below 1 kDa (*26*). Subsequently, the *lanA* gene encoding the peptide was cloned, and the peptide (mutacin 1140) was isolated and characterized as a 2263 Da posttranslationally modified peptide (Figure 1) (*1*). The small size described in earlier experiments suggested compact folding of the mutacin 1140 peptide. To further characterize this observation, we used a calibrated size-exclusion chromatography column and analyzed the apparent molecular mass of mutacin 1140 in 8 M urea, which was added to suppress oligomerization. The calculated relative size of the mutacin 1140 was below 1 kDa (Figure 2), suggesting a

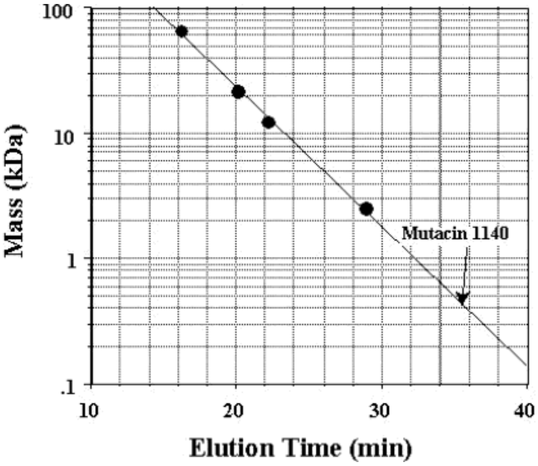

FIGURE 2: Size-exclusion chromotagraphy of mutacin 1140. The relative molecular size of mutacin 1140 was calculated based on the elution times of the standard polypeptides given in the Experimental Procedures.

tightly folded shape of the molecule that may contribute to the thermal stability of the peptide (*1*, *26*).

We then extended biophysical characterization to mass spectrometry. A doubly charged molecular ion of mutacin 1140 was subjected to MS/MS, yielding a complex spectrum of daughter ions. However, the major ion was the molecular ion, indicating the noteworthy stability of the peptide (results not shown). While this can be related to compact 3-D folding as suggested by size-exclusion chromatography studies, a possibility existed that intramolecular thioether bridges may also play a role (*1*, *2*). To test this hypothesis, we generated tryptic fragment (N-terminal residues 1−13 containing two thioether bridges) and subjected both the intact protein and this tryptic fragment to MS/MS under the same conditions. The results indicated high stability of the intact protein while the parent ion of the tryptic fragment completely dissociated. These data together suggest that mutacin 1140 is folded, which makes the molecule quite resistant to collision-induced dissociation in MS/MS experiments.

Mutacin 1140 contains several posttranslational modifications (Figure 1), including 3 dehydrated residues containing double bonds (e.g. Dha5, Dhb14, and Av22) (*1*, *2*). The double bonds could be selectively reduced at neutral pH with MeSH while leaving the thioether bridges intact. To test reactivity of these three residues, ESI-MS was used to evaluate the reaction products following reduction with MeSH at neutral pH. The data indicated that the major product is a molecule with one addition followed by molecules with two and then three additions. It was not clear whether the modifications were site-specific or statistically random. To determine the sites of modifications, the doubly charged ions of molecules with one and two modifications were subjected to MS/MS. The mass spectra of the daughter ions indicated that the mutacin 1140 with a single addition of MeSH had only a Dha5 modified residue, while the other two possible sites were not modified (Table 1). Mutacin 1140 with two additions had both Dha5 and Dhb14 and a small percentage of Av22 residues modified. These data suggest that MeSH reduction of mutacin 1140 begins with a site-specific modification of Dha5.

Overall, these data suggest that mutacin 1140 forms a folded compact structure. A folded conformation could explain the relatively small molecular mass determined by size-exclusion chromatography, the dissociation stability during MS/MS, as well as the differential reactivity of the

Table 1: Amino Acid Sequence of Mutacin 1140 and Daughter Ions Generated by Tandem Mass Spectrometry of the Doubly Charged Ion of Mutacin 1140 with One (*m*/*z* 1172) or Two (*m*/*z* 1211) Additions of 2-Mercaptoethanol (MeSH, at Neutral pH to Generate Additions Across Existing Double Bonds)[a]

amino acid position	one addition of MeSH		two additions of MeSH	
	b ions	y ions	b ions	y ions
Phe1				
Lys2	276 (1.6)		276 (1.6)	
Ala$_S$3	345 (1.1)		345 (0.7)	
Trp4		[1996][b] (1.2)	534 (0.7)	
Dha5	[678][c] ([0.6])	[1810] (1.1)	[678] ([1.5])	[1889] ([2.4])
Leu6	[791]/[824] ([1.2]/[0.5])		[791/825][d] ([0.8/2.3])	1664 [1742] (1.4 [1.4])
Ala$_S$7	[893] (1.3)	1551 (1.2)	[894] ([1.6])	[1630] ([1.8])
Abu$_S$8	[978]/[1012] ([3.8]/[1.7])	1442 (0.9)	[978/1012] ([7.6/1.6])	[1520, 1597] ([0.8, 1.6])
Pro9	[1074] ([2.9])	1364/1396 (4.9/0.6)	[1076/1108] ([3.3/5.8])	[1442, 1520] ([8.0, 0.8])
Gly10		1267 (1.0)	[1131/1164] ([6.2/9.1])	[1344] ([1.7])
Ala$_S$11	[1234] ([0.8])		[1232/1201] ([1.2/18.0])	[1287] ([0.7])
Ala12	[1305] ([1.3])		[1303] ([1.0])	[1186] ([7.1])
Arg13	[1462] ([2.7])	1036 (2.9)	[1462] ([3.0])	[1115] ([3.5])
Dhb14	[1544] ([2.0])		[1545 [1623]] ([2.9 [1.5]])	[957] ([2.8])
Gly15	[1600] ([1.7])	798 (1.1)	[1600 [1679]] ([1.8 [1.6]])	799 [874] (0.8 [1.6])
Ala$_S$16		741/772 (1.0/0.9)	[1671 [1747]/1701 [1781]] ([1.6 [1.6]/1.7/[1.4]])	742 (0.18)
Phe17		671 (0.4)	[1895/1929] ([1.3/1.4])	671 [749] (1.6 [0.8])
Asn18				
Ala$_S$19	[2000][b] ([2.0])			411 (1.6)
Tyr20				
Ala$_S$21				
Av22				

[a] Range was from 50 to 2000 *m*/*z*. Ions are listed according to their corresponding *m*/*z* numbers observed in the mass spectra. Av, aminovinyl cysteine. Relative intensities are shown in parentheses. [b] Daughter ions with *m*/*z* above 2000 are not detected by the mass spectrometer. [c] Ions with a gain of approximately 78 mass units are indicated with [ ]. [d] Ions with a gain or loss of approximately 32 or 33 mass units, respectively, are indicated after /.

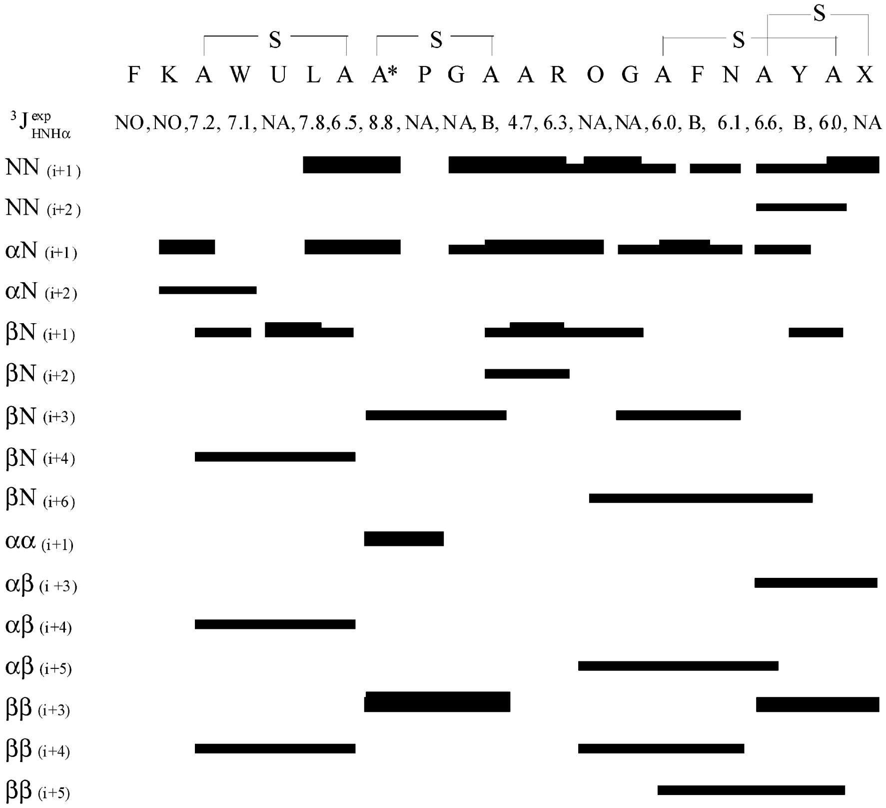

FIGURE 3: Summary of the NOEs and *J* couplings from the NMR data: short- ($x < 2.9$ Å), medium- (2.9 Å $\leq x \leq$ 3.4 Å), and long- ($x > 3.4$ Å) range NOE cross-peaks, and the height of the bars indicates the magnitude of the interaction. The following one letter abbreviations represent: alanyl moieties of a lanthionine (A-S-A), 2,3-didehydroalanine (U), 2-aminobutyric acid moiety of a methyl-lanthionine (A*), 2,3-didehydrobutyrine (O), and amino vinyl moiety of the *S*-amino vinyl-D-cysteine (X). Values of $^3J_{NHH\alpha}$ couplings are in Hz. Some couplings were not observed because of exchange (NO), not applicable due to unsaturated amino acids (NA) or too broad to accurately measure (B).

dehydrated residues. However, a more detailed understanding of the 3-D structure of mutacin 1140 and its properties important for biological activity required nuclear magnetic resonance studies.

Mutacin 1140 Has Several Long-Range NOEs. Interproton distances were determined from NOE volumes measured from 2-D NMR NOESY spectra. A total of 49 interresidue restraints were measured including 32 sequential, 10 medium-range ($1 < i \leq 3$), and 7 long-range NOEs ($i > 3$) (Figure 3). Long-range NOEs are particularly important in defining the native conformation. Because previous structural studies of lantibiotics did not report NOEs spanning thioether rings, we paid particular attention to the validity of these measurements. The long-range NOEs were seen with all NOESY mixing times, indicating that they were not the result of spin diffusion. Additionally, the location of the long-range NOEs spanning the thioether rings complement each other, given that they are all generally present in the same region of the peptide.

Mutacin 1140 Has an Ensemble of Several 3-D Structures. The NOE volumes were converted to internuclear distances as described above, and the NOE distances were used to limit the available conformational space of the molecule to experimentally relevant areas during the molecular dynamic (MD) simulations. Extensive restrained molecular dynamic (RMD) simulations were undertaken to explore the conformational space to find all conformations that are consistent with experimental data. Two-hundred structures evenly spaced in time from the RMD simulation were energy minimized. These energy minimized conformations were clustered into families using the computer program XCluster (*25*). The clustering was done by comparing the backbone ϕ and ψ dihedral angles of the amino acids in each of the 200 energy minimized conformations. All clustered families with a population of four or more conformations (≥2% of the total) were considered for further analysis. Using these criteria, 11 families were identified with a total of 95 energy minimized structures. The largest family was composed of 22 structures (11% of the total conformations), and a representative structure was determined from each family by XCluster (Figure 4). The 11 representative structures from each family were superimposed, and the RMS deviation was 4.2 Å for all atoms and 2.8 Å for the backbone atoms. The overall backbone structure is horseshoe-shaped. Rings A and B are on one side, and the intertwined rings C and D are positioned on the other side.

Ensemble of Structures Is in Good Agreement with Experimental Data. The 200 energy minimized conformations were in good agreement with the 49 distance restraints used during the RMD simulations. The 200 energy minimized structures were checked for NMR restraint violations using PROCHECK-NMR software (*24*), which measured the average distances between the restrained nuclei from all the 200 energy minimized conformations. Lower- and upper-bound limits used to test the 49 distance restraints were determined by adding and subtracting 1.0 Å to the calculated NOE-derived distances; no violations were said to have occurred if these average distances were between these limits.

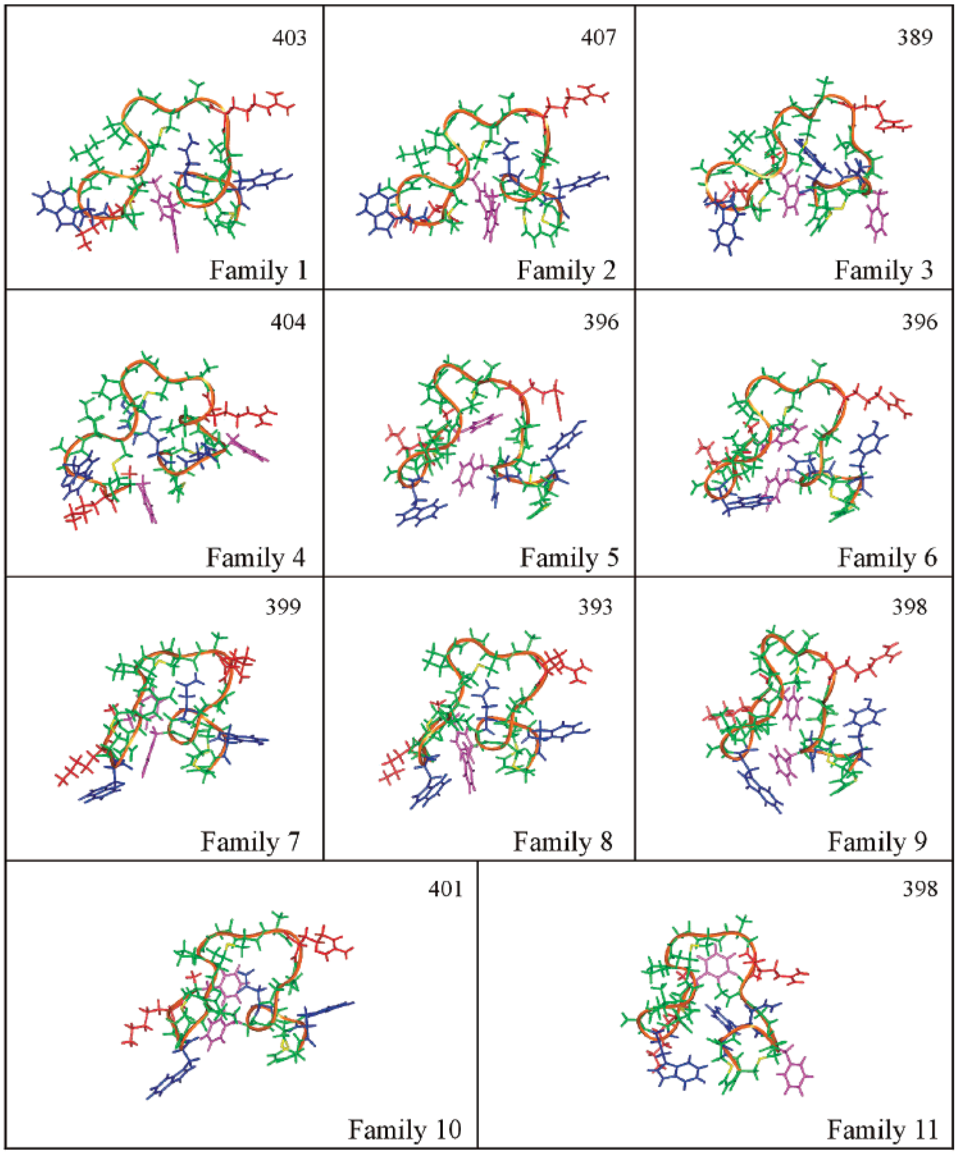

FIGURE 4: Representative structures determined by XCluster for each family. Structures are shown in the same relative orientation for clarity. The energies (kcal) of each of these minimized structures are listed in top right corner. The phenylalanines, charged residues, and polar residues are pink, red, and blue, respectively. The ribbon traces the backbone atoms. The four rings can be visualized from the backbone trace and from the thioether linkages (yellow). Green represents the nonaromatic hydrophobic residues.

A total of four restraint violations, none greater than 0.2 Å, were found. The small violations were found between Ala$_S$3 H$^{\beta*}$ and $_S$Ala7 H^N, Abu$_S$8 H$^\beta$ and $_S$Ala11 H^N, Dhb14 H$^\beta$ and Ala$_S$19 H$^\alpha$, and Tyr20 H$^{\beta*}$ and $_S$Ala21 H^N.

Given that the NOE restraints were used in the modeling, agreement between the RMD simulation and the experiment was more a test for the computer modeling than for the validity of the ensemble of structures. Therefore, we also measured ${}^3J^{\mathrm{exp}}_{\mathrm{HNH}\alpha}$ couplings and compared the results to calculated values, ${}^3J^{\mathrm{calc}}_{\mathrm{HNH}\alpha}(\phi)$, and population-weighted values, ${}^3J^{\mathrm{av}}_{\mathrm{HNH}\alpha}(\phi)$, as described above. The *J* couplings were not used as restraints in the RMD simulations and thus can provide a good validation of the simulation.

The experimental ${}^3J^{\mathrm{exp}}_{\mathrm{HNH}\alpha}$ scalar coupling values are listed in Figure 3. Table 2 gives the quality value *Q* between ${}^3J^{\mathrm{exp}}_{\mathrm{HNH}\alpha}$ and either individual ${}^3J^{\mathrm{calc}}_{\mathrm{HNH}\alpha}(\phi)$ or ${}^3J^{\mathrm{av}}_{\mathrm{HNH}\alpha}(\phi)$. The agreement between experimental couplings and computational values was best when the comparison was with the entire population-weighted ensemble of structures (whose calculated couplings are represented by ${}^3J^{\mathrm{av}}_{\mathrm{HNH}\alpha}(\phi)$) and not

Table 2: Quality Values for Experimental versus Calculated *J* Couplings

family	% size of family	*Q* (Hz^2)^a
1	9.5	12.5
2	12.6	15.1
3	4.2	15.8
4	9.5	19.2
5	17.9	19.0
6	4.2	23.3
7	4.2	16.0
8	4.2	11.9
9	4.2	15.3
10	23.2	13.7
11	6.3	14.4
all	100	11.8

^{a} $Q = \sum_{i=1}^{\mathrm{Nres}} |{}^3J^{\mathrm{exp}}_{\mathrm{HNH}\alpha} - {}^3J^{\mathrm{calc}}_{\mathrm{HNH}\alpha}|$ for all individual family members (1−11) or $Q = \sum_{i=1}^{\mathrm{Nres}} |{}^3J^{\mathrm{exp}}_{\mathrm{HNH}\alpha} - {}^3J^{\mathrm{av}}_{\mathrm{HNH}\alpha}|$ for the population-weighted average (all).

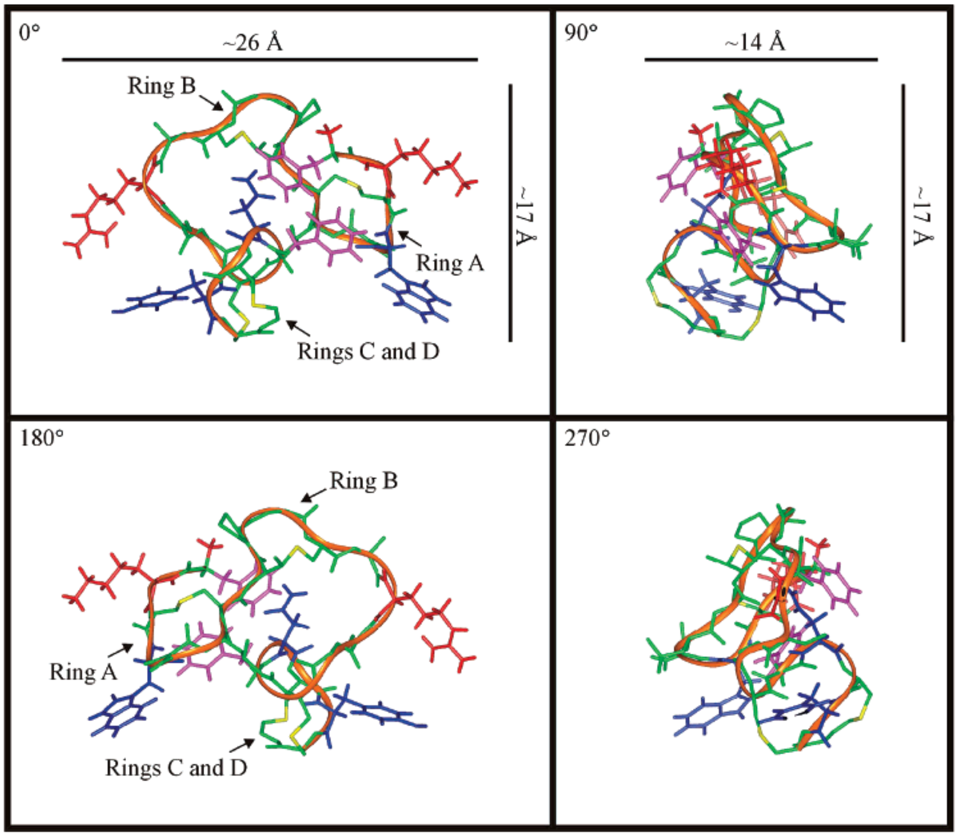

FIGURE 5: Representative structure of the largest family. The dimensions of this structure is 26 × 17 × 14 Å. Side chains are only shown for the phenylalanines (pink), charged residues (red), and polar residues (blue). The orange ribbon traces the backbone atoms. The four rings can be visualized from the backbone trace and from the thioether linkages (yellow). The green color represents the nonaromatic hydrophobic residues. The structures shown were rotated around the *y*-axis by 90°.

with individual structures. This strongly suggested that the ensemble of conformations produced during the restrained molecular dynamic simulation was a good representation of the true ensemble of structures of mutacin 1140 in solution.

Mutacin 1140 Is Comprised of Rigid Rings Connected by Flexible Linkers. The analysis that follows focused on the representative structures from each family in the ensemble of structures (Figure 4). The overall shape of the representative structure from the largest family, shown in Figure 5, was approximately 26 Å in length, 17 Å in diameter, and 14 Å in width. Over 72% (16 out of the 22 residues) of the residues in mutacin 1140 were part of one of the four thioether rings, and these rings constitute structurally well-defined elements. Ring A was made from five residues, $_{\mathrm{D}}$Ala$_{\mathrm{S}}$3-Trp4-Dha5-Leu6-$_{\mathrm{S}}$Ala7. Ring B was composed of four residues, Abu$_{\mathrm{S}}$8-Pro9-Gly10-$_{\mathrm{S}}$Ala11. Rings C and D were intertwined and composed of residues $_{\mathrm{D}}$Ala$_{\mathrm{S}}$16-Phe17-Asn18-$_{\mathrm{D}}$Ala$_{\mathrm{S}}$19-Tyr20-$_{\mathrm{S}}$Ala21 for ring C and $_{\mathrm{D}}$Ala$_{\mathrm{S}}$19-Tyr20-$_{\mathrm{S}}$Ala21-Avi (the amino vinyl terminus) for ring D. The central hinge region had four flexible residues, Ala12-Arg13-Dhb14-Gly15, which connected rings A and B to rings C and D.

A global representation of mutacin 1140 dynamics is shown in Figure 6. Some residues—especially 2, 6, 8, 16, 19, and 20—were rigid and did not experience fluctuations on the time scale of the RMD simulation. Others—most notably 4 and 5, 9 and 10, 14 and 15, and 18 and 19—underwent concerted motions. With the exception of residues 14 and 15, all of the pairs that show concerted motions were in thioether rings and were situated opposite to the sulfur atom linkage. Finally, some residues—7, 8, 12, 14, 15, 18, and19—underwent rapid large-scale fluctuations (correlated or not) that indicate significant flexibility. Details on each region are given below.

Ring A. No typical β turns, γ turns, or hydrogen bonds were found in this lanthionine ring (Figure 7a). The RMS deviation for ring A was 1.9 Å for all atoms and 0.8 Å for the backbone atoms. A considerable amount of concerted motion in the ψ angle of Trp4 and the ϕ angle of Dha5 occurred during the RMD simulation (Figures 6 and 7a). The movement of these dihedral angles allows for a conformational change that alters the orientation of amide proton of Dha5, which can either protrude toward the solvent or be directed toward the interior of the ring. However, the Dha5 vinyl side chain remains extended out into the solvent and did not get not buried in the ring.

The Z−H$^{\beta}$ proton of Dha5 underwent a chemical shift change of almost 0.3 ppm when the acetonitrile concentration changed from 70 to 90%, while the Dha5 E−H$^{\beta}$ chemical shift changed by only 0.03 ppm in the same solvent systems (Figure 8a). This is likely the result of diamagnetic anisotropy of a neighboring aromatic ring. The extent and the direction of the change in chemical shift depends on the orientation and the distance of the aromatic ring from the proton. Thus, the orientation and distance of the Trp4 side chain with respect to the Dha5 vinyl protons probably shifts with varying acetonitrile concentrations. The average distance between the aromatic ring of Trp4 to the Z−H$^{\beta}$ and E−H$^{\beta}$ of Dha5 was 7.3 and 7.5 Å, respectively. These distances do not fully

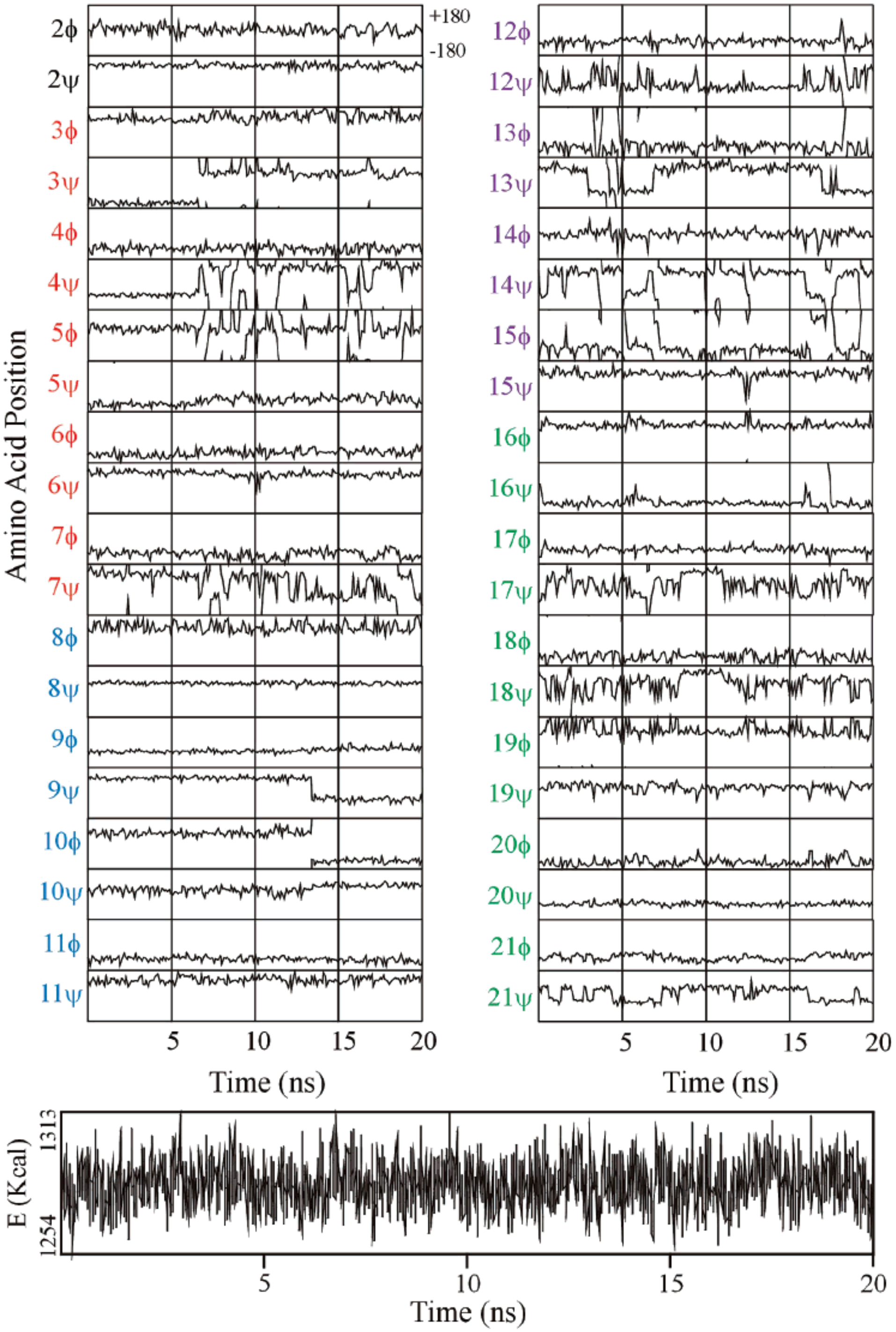

FIGURE 6: Backbone dihedral angles of each amino acid are plotted vs time in the 20 ns molecular dynamic simulation. In addition, the energies of the molecular dynamic simulation are given below. The colors indicating amino acids are red (ring A), blue (ring B), purple (central hinge), and green (rings C and D).

explain why one proton is affected significantly by the ring current of Trp4, while the other one is not. However, there were several conformations in which the tryptophan ring was significantly closer to the Z−H$^{\beta}$ than to E−H$^{\beta}$, and one of those conformations is shown in Figure 8a along with the distance plots of the aromatic ring of Trp4 to the Z−H$^{\beta}$ and E−H$^{\beta}$ of Dha5.

In addition, the ψ bond of $_{S}$Ala7, which is not confined by the thioether ring, can freely rotate (Figures 6 and 7a). This motion allows ring A to spin freely with respect to ring B and has not been described in any other type A lantibiotic. The rotational flexibility around this bond may be important for orienting these rings into their functional orientation in the membrane.

Ring B. This 2-methyl-lanthionine ring forms the most well-defined structural element in mutacin 1140 (Figure 7a). The RMS deviation of this ring was 0.9 Å for all atoms and 0.7 Å for the backbone atoms. The amide proton of $_{S}$Ala11 was detectable for 55 min during a deuterium exchange experiment, and all other amide protons were fully exchanged before our first measurement (∼2 min). This is evidence of a hydrogen bond, and from the 3-D structure the hydrogen

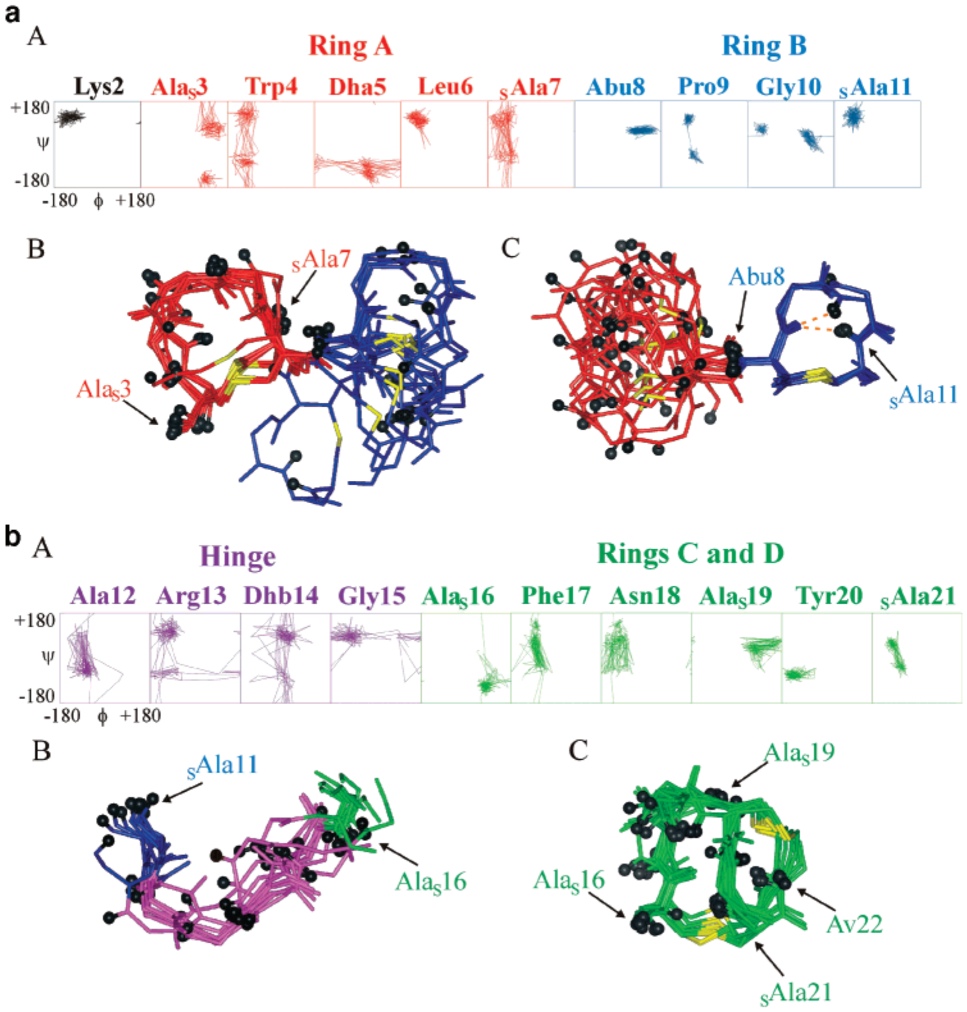

FIGURE 7: Structural summary of mutacin 1140. The (ϕ,ψ) plots are given for each residue and represent the RMD trajectory. The molecular models are superimpositions of the representative energy minimized structure from each of the 11 major families. In panel a, rings A and B are shown with ring A superimposed (left) and with ring B superimposed (right). This indicates that the rings are relatively rigid but move relative to one another. In panel b, the central hinge region is shown on the left, and the intertwined rings C and D are on the right. For all molecular models, thioether linkages are shown in yellow, amide protons are black balls, and the dashed orange lines represent hydrogen bonding.

bond is seen between the $_{S}$Ala11 amide proton and the Abu$_{S}$8 carbonyl oxygen (Figure 7a).

There were two conformations found in ring B during the molecular dynamic simulation. These resulted from the motion of the ψ bond of Pro9 and the ϕ bond of Gly10. The four residues in this ring formed either a type I or a type II β turn structure. As is often found for type I and type II β turns, Pro9 and Gly10 are in positions 2 and 3. In the type II β turn structure, the amide proton of Gly10 is directed toward the interior of the ring. In this conformation, Gly10 may be involved in forming a bifurcated hydrogen bond between the amide protons of Gly10 and $_{S}$Ala11 to the carbonyl oxygen atom of Abu$_{S}$8, as was reported for nisin (*7*). The formation of the type II β turn and the hydrogen bond between the $_{S}$Ala11 amide proton and the Abu$_{S}$8 carbonyl oxygen have also been reported in similar rings found in gallidermin (*5*, *7*). In the type I β turn structure, the amide proton of Gly10 is directed toward the solvent. The interconversion between the type I β turn to a type II β turn has not been described in other lantibiotics.

Central Hinge Region. Figures 6 and 7b indicate a large amount of flexibility in residues 12−15. This region deviates considerably from an extended conformation and has a significant population of type V β turn ($\phi_{i+1} = -80°$, $\psi_{i+1} = 80°$, $\phi_{i+2} = 80°$, and $\psi_{i+2} = -80°$) that folds the N-terminal rings AB toward the C terminal intertwined rings CD, generating the horseshoe-like structure (Figure 7b). Several long-range NOEs were found outside of the thioether ring structures in this central hinge region (Figure 3); these long-range NOEs have not been reported before in nisin and gallidermin. Of particular importance for the type V β turn formation were NOEs from Asn18 H$^{\beta}$, Ala$_{S}$19 H$^{\alpha}$, and Tyr20 H^{N} to Dhb14 H$^{\beta}$. In addition, there were long-range NOEs between Ala$_{S}$11 H$^{\beta}$ and Arg13 H^{N} and between Gly15 H^{N} and Asn18 H$^{\beta}$. These long-range NOEs helped define the turn-like motif found in this region. There is also a considerable amount of flexibility within this region, which is characteristic of a type A lantibiotic. This flexibility has been suggested by mutagenesis studies in other lantibiotic systems to be important for lantibiotic activity (*27*−*29*).

Intertwined Rings C and D. Like ring A, no regular turns or hydrogen bonds were found in rings C and D (Figure 7b). As in gallidermin, the two intertwined rings formed a rigid well-defined structure. The RMS deviation of these rings was

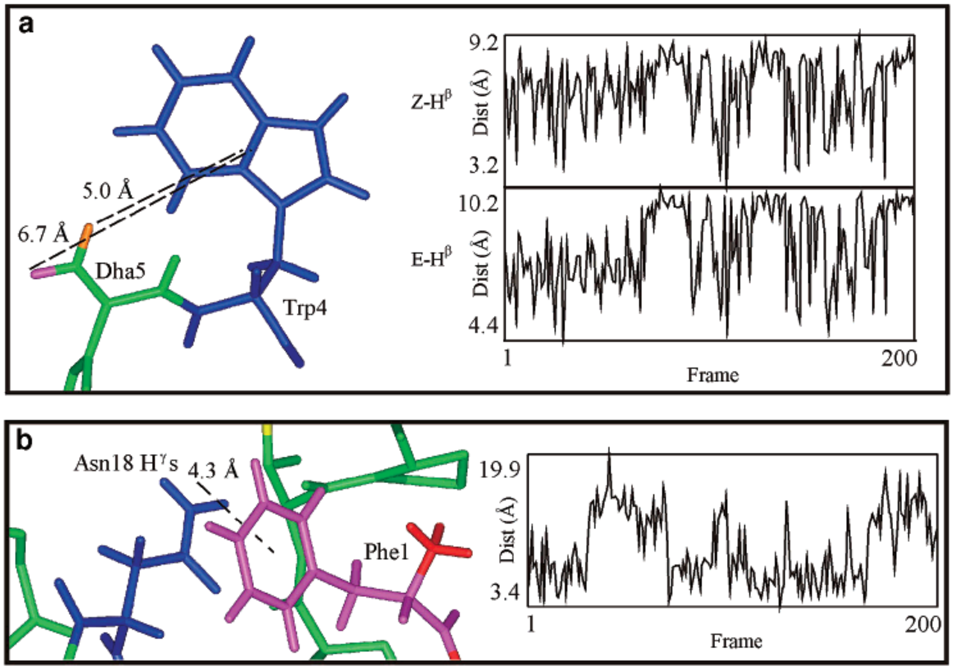

c

CD_3CN:H2O Concentration	90%	80%	70%
Dha5 vinyl Z-H$^{\beta}$ (ppm)	5.89	5.68	5.61
Dha5 vinyl E-H$^{\beta}$ (ppm)	5.38	5.36	5.35
Asn18 H$^{\gamma}$s (ppm)	6.4	6.57	6.61

FIGURE 8: Representation of the ring current shift seen in mutacin 1140. (a) Z$-$H$^{\beta}$ (orange) of Dha5 shifted nearly 0.3 ppm, while E$-$H$^{\beta}$ (pink) was only slightly affected. In the conformation shown, Dha5 Z$-$H$^{\beta}$ is 5 Å from the aromatic ring of Trp4, while Dha5 E$-$H$^{\beta}$ is 6.7 Å. The distance plots show the distances between the nuclei during the RMD simulation. (b) The H$^{\delta}$s of Asn18 shifts slightly over 0.2 ppm, presumably because of the ring current of Phe1. In the conformation shown, Asn18 H$^{\delta}$s are only 4.3 Å from the aromatic ring of Phe1 in this representative structure. The distance plots show the distances between the nuclei during the RMD simulation. (c) Chemical shifts of these protons in varying acetonitrile concentrations.

1.9 Å for all atoms and 0.8 Å for backbone atoms. Asn18 H$^{\delta}$s, which are overlapped and degenerate, underwent a chemical shift change of 0.2 ppm when the acetonitrile concentration was changed from 70 to 90% (Figure 8c). As described earlier for the Dha5 vinyl protons, the diamagnetic anisotropy of a neighboring aromatic ring is a likely cause for this effect. From the primary sequence, Phe17 or Tyr20 would seem to be most likely candidates as sources of the ring current shift, but from the 3-D structures these rings are too far away to elicit the chemical shift change seen in the Asn18 H$^{\delta}$s. However, Phe1 actually appears to be the most likely mediator of this effect. The average distance between the aromatic ring of Phe1 and Asn18 H$^{\delta}$s was 7.2 Å. However, there were conformations in which the distance between the aromatic ring of Phe1 and the H$^{\delta}$s of Asn18 were less than 4.5 Å apart, and one of those conformations is shown in Figure 8b along with the distance plots of the aromatic ring of Phe1 to Asn18 H$^{\delta}$s. In addition, the molecular dynamic simulation showed a considerable amount of motion in the ψ angles of Phe17 and Asn18 (Figures 6 and 7b). This motion caused a similar conformational change of the amide protons of Asn18 and Ala$_S$19 as previously described for Dha5 and Gly10. However, the motion of these two dihedral angles also allows for a considerable amount of motion for the Asn18 side chain. Asparagine residues have been shown to be very important for complex formation in other transmembrane peptides (*30*, *31*). The internal motion of this region may aid in intermolecular hydrogen bond formation when inserted into the membrane bilayer.

DISCUSSION

Both size-exclusion chromatography and mass spectrometry experiments suggest that mutacin 1140 forms a compact structure, thus supporting and complementing the NMR data. Mutacin 1140 has been characterized as a 2263 Da post-translationally modified peptide (*1*, *2*). However, the apparent relative size of mutacin 1140 was calculated by size-exclusion chromatography to be less than 1 kDa. In addition, the increased MS/MS stability of mutacin 1140, as compared to the tryptic fragments, further suggests that the 3-D structure of mutacin 1140 makes the molecule more resistant to collision-induced dissociation. Furthermore, the site-specific reduction of the three double bonds present in mutacin 1140 could be explained from the 3-D structure. The first residue to be reduced is Dha5 followed by the reduction of Dhb14 and/or Av22. The vinyl group of Dha5 protrudes out from ring A, making it more accessible to MeSH reduction than the Dhb14 residue that is part of the

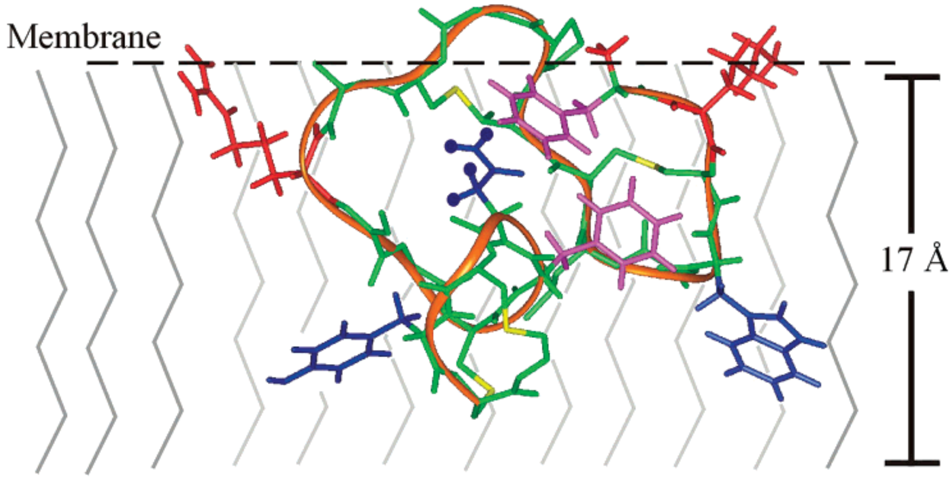

FIGURE 9: Model of membrane-bound mutacin 1140. The type II β turn structure found in ring B is positioned at the surface of the membrane. This allows us to determine the position of the charged amino terminus, the Lys2 side chain, and the Arg13 side chain into a common plane that could associate with the negative charge headgroups and anchor the molecule to the surface of the membrane. The polar side chain of asparagine, which is represented by a ball-and-stick, is submerged into the bilayer. In this orientation, the asparagine residue is easily accessible for complex formation. The Trp4 side chain is positioned away from the rest of the molecule and may help in oligomerization specificity. Given the dimensions of mutacin 1140, this monomer would span ~15 Å into the lipid bilayer.

turn-like motif found in the hinge region. Overall, it appears that the unique features of the 3-D structure of mutacin 1140 contribute to the increased physical stability of this antibacterial peptide.

The 3-D global structures of mutacin 1140 all are horseshoe-shaped. The overall high RMS deviation of these structures was largely due to the rotation around the ψ angle of sAla7 and from the flexibility seen in the residues that make up the hinge region. However, when these structures were superimposed, the thioether rings were generally in the same area. The structures were supported by several long-range NOEs that were found between residues of the hinge region to those of the intertwined rings C and D. Further evidence for this bent conformation came from chemical shift changes in Asn18 H^{δ} when the acetonitrile concentration changed from 70 to 90%, which are believed to be the result of diamagnetic anisotropy of a neighboring aromatic ring. From the 3-D structures, Phe1 appears to be the likely source of this effect.

The structure of mutacin 1140 differs from the structure determined for gallidermin (*5*). Gallidermin was found to have an elongated screw-like shape and a well-defined structure with an RMS deviation of 1.7 Å for the backbone atoms, but no long-range NOEs were described for the gallidermin structural calculations and only the sequential NOE connectivities were shown. However, modeling studies in which the gallidermin−trypsin interaction was examined showed that gallidermin adopted a bent structure to fit into the catalytic cleft of the trypsin enzyme (*32*). Our mutacin 1140 structures resemble the structures of gallidermin when complexed to trypsin. Furthermore, a reduction in trypsin cleavage activity of gallidermin was shown to occur when a bulky residue was placed (e.g., A12L) in the hinge region. This loss of this activity was attributed to a decrease in the flexibility of the hinge region, which would prevent gallidermin from forming this bent conformation (*29*). Given the structure of mutacin 1140, the loss of activity is more likely to be attributed to the disruption of the reverse turn in the hinge region.

Structural analyses of nisin have shown that local structural elements are affected by bringing the molecule from an aqueous solution to a membrane-like environment, whereas the global structure essentially remains the same (*7*). In nisin, one of the most profound structural element changes was seen with the amide proton of Dha5. The amide proton was directed toward the interior of the ring when nisin was complexed to micelles and protruded from the ring when it was solvent exposed. The authors noted that the likely reason for this conformational change is due to an interaction of Dha5 with the micelles and that the conformation of the amide proton of Dha5 protruding into the ring appears to be energetically favored in the lipid environments. This conformational change of the amide protons may be a common feature among other residues confined by thioether rings. In ring A of mutacin 1140, the concerted motion of the ψ angle of Trp4 and the ϕ angle of Dha5 allows the amide proton of Dha5 to either be directed toward the interior of the ring or the solvent. Additionally, the Gly10 amide proton of the nisin micelle complexes was shown to be directed toward the interior of ring B, forming a bifurcated hydrogen bond between the amide proton of Gly10 and $_{S}$Ala11 to the carbonyl oxygen atoms of Abu$_{S}$8. This conformation forms a type II β turn structure, which was also seen in the mutacin 1140 structures. However, during a long molecular dynamic simulation, the ψ angle of Pro9 and the ϕ angle of Gly10 in mutacin 1140 had two distinct conformations. The amide proton of Gly10 was capable of flipping out from the interior of the ring exposing itself to solvent. In this conformation, the four residues that comprise ring B of mutacin 1140 form a type I β turn structure. The flipping of the amide proton from solvent to the interior of the ring was also seen during the molecular dynamic simulation for the Asn18 and Ala$_{S}$-19 residue in mutacin 1140. Burying of amide protons into the thioether rings may be a common feature among membrane-bound lantibiotics, given that these small structural element changes in nisin have been described and that the 3-D structures of mutacin 1140 suggests that the same small structural element changes can occur.

The structure determined in this study is consistent with biological properties. When Dha5 in nisin was replaced by alanine, the resulting lantibiotic had wild-type activity against vegetative cells but was less active as an inhibitor of spore outgrowth (*33*). Little is known about the function of inhibiting spore outgrowth, but it is believed that the double bond in Dha5 provides a reactive group for the interaction with a spore-associated factor that is essential for outgrowth (*34*). Therefore, to be able to inhibit spore outgrowth, the vinyl group must be positioned in such a way that it is accessible to the spore-associated factor. The vinyl protons of Dha5 in mutacin 1140 are rigidly oriented toward the solvent and could easily interact with the spores with no conformational change. This accessible orientation has been seen in the lantibiotic nisin and suggests that this conformation may be required for inhibition of spore outgrowth (*7*).

In studies with other membrane-associated peptides, researchers have found that an asparagine side chain is essential for mediating the association of transmembrane peptides (*31*). The fact that asparagine residues are capable of being simultaneous hydrogen bond donors and acceptors makes them important for the formation of homo- or hetero-oligomers. Interestingly, an asparagine residue is found at position 18 in the lantibiotics epidermin, gallidermin, staphylococcin T, mutacin b-NY266, and mutacin 1140. Lantibiotics are too small to form transmembrane pores on their own. Therefore, complex formation is essential for pore formation, and from the 3-D structure of mutacin 1140, the asparagine side chain is accessible for interresidue hydrogen bonding.

The structure determined in this study is the first step toward understanding how mutacin 1140 interacts with the membrane. Given that the global structure of nisin essentially remains the same when bound to micelles (*7*), the 3-D structure of mutacin 1140 determined in acetonitrile/water (80:20) is a reasonable starting point to predict the orientation of the membrane-bound molecule. Reverse turns are normally located at the surface of the membrane. Therefore, the type II β turn structure found in ring B might be positioned at the surface (Figure 9). This orientation is further supported by the position of the charged amino terminal, Lys2 side chain, and Arg13 side chain. In this orientation, these positive charged residues could associate with the negatively charged headgroups of the lipids, anchoring the molecule on the surface of the membrane. Additionally, asparagine residues rarely occur on the lipid exposed surface (*30*). In this membrane-bound model, the asparagine residue is submerged into the lipid bilayer, providing a strong thermodynamic driving force for the complex formation activity found in this residue. In addition, tryptophan residues have been shown to possess antiaggregation properties (*35*). In this model, the Trp4 side chain is directed away from the rest of molecule and may be important for oligomerization specificity by preventing mutacin 1140 from aggregating. Validation of this model will require further experimental structural data in a membrane environment.

ACKNOWLEDGMENT

NMR data were collected at the Advanced Magnetic Resonance Imaging and Spectroscopy (AMRIS) Facility in the McKnight Brain Institute of the University of Florida. Chemical sequencing was collected at the Interdisciplinary Center for Biological Research at the University of Florida, and the mass spectrometric data were collected at the University of Alabama. The PE-Sciex API III mass spectrometer was purchased by funds from a NIH Instrumentation grant (S10RR06487) and from UAB. Operation of the UAB Comprehensive Cancer Center Mass Spectrometry Shared Facility has been supported in part by a NCI Core Research Support grant to the UAB Comprehensive Cancer (P30 CA13148). We thank Marion Kirk and Stephen Barnes for their expert assistance and advice.

REFERENCES

1. Hillman, J. D., Novak, J., Sagura, E., Gutierrez, J. A., Brooks, T. A., Crowley, P. J., Hess, M., Azizi, A., Leung, K. P., Cvitkovitch, D., and Bleiweis, A. S. (1998) Genetic and biochemical analysis of mutacin 1140, a lantibiotic from *Streptococcus* mutans, *Infect. Immun. 66*, 2743−2749.
2. Smith, L., Novak, J., Rocca, J., McClung, S., Hillman, J. D., and Edison, A. S. (2000) Covalent structure of mutacin 1140 and a novel method for the rapid identification of lantibiotics, *Eur. J. Biochem. 267*, 6810−6816.
3. vanDeVen, F. J. M., and Jung, G. (1996) Structures of lantibiotics studied by NMR, *Antonie van Leeuwenhoek Int. J. Gen. Mol. Microbiol. 69*, 99−107.
4. Kellner, R., Jung, G., Horner, T., Zahner, H., Schnell, N., Entian, K. D., and Götz, F. (1988) Gallidermin—a new lanthionine-containing polypeptide antibiotic, *Eur. J. Biochem. 177*, 53−59.
5. Freund, S., Jung, G., Gutbrod, O., Folkers, G., Gibbons, W. A., Allgaier, H., and Werner, R. (1991) The solution structure of the lantibiotic gallidermin, *Biopolymers 31*, 803−811.
6. Schnell, N., Entian, K. D., Schneider, U., Götz, F., Zahner, H., Kellner, R., and Jung, G. (1988) Prepeptide sequence of epidermin, a ribosomally synthesized antibiotic with four sulfide rings, *Nature 333*, 276−278.
7. van den Hooven, H. W., Doeland, C. C. M., vandeKamp, M., Konings, R. N. H., Hilbers, C. W., and vandeVen, F. J. M. (1996) 3-D structure of the lantibiotic nisin in the presence of membrane-mimetic micelles of dodecylphosphocholine and of sodium dodecylsulphate, *Eur. J. Biochem. 235*, 382−393.
8. van den Hooven, H. W., Spronk, C., vandeKamp, M., Konings, R. N., Hilbers, C. W., and vandeVen, F. J. M. (1996) Surface location and orientation of the lantibiotic nisin bound to membrane-mimicking micelles of dodecylphosphocholine and of sodium dodecylsulphate, *Eur. J. Biochem. 235*, 394−403.
9. van den Hooven, H. W., Fogolari, F., Rollema, H. S., Konings, R. N., Hilbers, C. W., and van deVen, F. J. M. (1993) NMR and circular dichroism studies of the lantibiotic nisin in nonaqueous environments, *FEBS Lett. 319*, 189−194.
10. van de Ven, F. J. M., vandenHooven, H. W., Konings, R. N. H., and Hilbers, C. W. (1991) NMR Studies of lantibiotics—the structure of nisin in aqueous solution, *Eur. J. Biochem. 202*, 1181−1188.
11. Chan, W. C., Bycroft, B. W., Leyland, M. L., Lian, L. Y., Yang, J. C., and Roberts, G. C. K. (1992) Sequence-Specific Resonance Assignment and Conformational Analysis of Subtilin by 2-D NMR, *FEBS Lett. 300*, 56−62.
12. Abee, T. (1995) Pore-forming bacteriocins of gram-positive bacteria and self-protection mechanisms of producer organisms, *FEMS Microbiol. Lett. 129*, 1−9.
13. Montville, T. J., and Chen, Y. (1998) Mechanistic action of pediocin and nisin: recent progress and unresolved questions, *Appl. Microbiol. Biotechnol. 50*, 511−519.
14. Breukink, E., Wiedemann, I., van Kraaij, C., Kuipers, O. P., Sahl, H. G., and de Kruijff, B. (1999) Use of the cell wall precursor lipid II by a pore-forming peptide antibiotic, *Science 286*, 2361−2364.
15. Breukink, E., Bonev, B. B., Wiedemann, I., Sahl, H. G., Watts, A., and de Kruijff, B. (2001) Specific interaction of the lantibiotic nisin with lipid II leads to highly efficient pore formation, *Biophys. J. 80*, 7.
16. Moll, G. N., Roberts, G. C. K., Konings, W. N., and Driessen, A. J. M. (1996) Mechanism of lantibiotic-induced pore formation, *Antonie van Leeuwenhoek Int. J. Gen. Mol. Microbiol. 69*, 185−191.

17. Braunschweiler, L., and Ernst, R. R. (1983) Coherence Transfer by Isotropic Mixing—Application to Proton Correlation Spectroscopy, *J. Magn. Reson. 53*, 521−528.
18. Kumar, A., Ernst, R. R., and Wüthrich, K. (1980) A 2-D nuclear Overhauser enhancement (2-D NOE) experiment for the elucidation of complete proton−proton cross relaxation networks in biological macromolecules, *Biochem. Biophys. Res. Commun. 95*, 1−6.
19. Karplus, M. (1959) Contact electron-spin coupling of nuclear magnetic moments, *J. Chem. Phys. 30*, 11−15.
20. Edison, A. S., Markley, J. L., and Weinhold, F. (1994) Calculations of One-Bond, Two-Bond, and Three-Bond Nuclear Spin−Spin Couplings in a Model Peptide and Correlations with Experimental Data, *J. Biomol. NMR 4*, 519−542.
21. Johnson, B. A., and Blevins, R. A. (1994) NMR View—a Computer Program for the Visualization and Analysis of NMR Data, *J. Biomol. NMR 4*, 603−614.
22. Allgaier, H., Jung, G., Werner, R. G., Schneider, U., and Zahner, H. (1986) Epidermin—Sequencing of a Heterodet Tetracyclic 21-Peptide Amide Antibiotic, *Eur. J. Biochem. 160*, 9−22.
23. Skaugen, M., Nissenmeyer, J., Jung, G., Stevanovic, S., Sletten, K., Abildgaard, C. I. M., and Nes, I. F. (1994) *In vivo* conversion of L-serine to D-alanine in a ribosomally synthesized polypeptide, *J. Biol. Chem. 269*, 27183−27185.
24. Laskowski, R. A., Rullmann, J. A. C., MacArthur, M. W., Kaptein, R., and Thornton, J. M. (1996) AQUA and PROCHECK-NMR: Programs for checking the quality of protein structures solved by NMR, *J. Biomol. NMR 8*, 477−486.
25. Shenkin, P. S., and McDonald, D. Q. (1994) Cluster analysis of molecular conformations, *J. Comput. Chem. 15*, 899−916.
26. Hillman, J. D., Johnson, K. P., and Yaphe, B. I. (1984) Isolation of a *Streptococcus* Mutans Strain Producing a Novel Bacteriocin, *Infect. Immun. 44*, 141−144.
27. Kuipers, O. P., Rollema, H. S., Beerthuyzen, M. M., Siezen, R. J., and deVos, W. M. (1995) Protein engineering and biosynthesis of nisin and regulation of transcription of the structural nisA gene, *Int. Dairy J. 5*, 785−795.
28. Kuipers, O. P., Bierbaum, G., Ottenwalder, B., Dodd, H. M., Horn, N., Metzger, J., Kupke, T., Gnau, V., Bongers, R., van den Bogaard, P., Kosters, H., Rollema, H. S., deVos, W. M., Siezen, R. J., Jung, G., Götz, F., Sahl, H. G., and Gasson, M. J. (1996) Protein engineering of lantibiotics, *Antonie van Leeuwenhoek Int. J. Gen. Mol. Microbiol. 69*, 161−169.
29. Ottenwalder, B., Kupke, T., Brecht, S., Gnau, V., Metzger, J., Jung, G., and Götz, F. (1995) Isolation and characterization of genetically engineered gallidermin and epidermin analogues, *Appl. Environ. Microbiol. 61*, 3894−3903.
30. Choma, C., Gratkowski, H., Lear, J. D., and DeGrado, W. F. (2000) Asparagine-mediated self-association of a model transmembrane helix, *Nat. Struct. Biol. 7*, 161−166.
31. Zhou, F. X., Merianos, H. J., Brunger, A. T., and Engelman, D. M. (2001) Polar residues drive association of polyleucine transmembrane helices, *Proc. Natl. Acad. Sci. U.S.A. 98*, 2250−2255.
32. Jung, G. (1991) Lantibiotics—ribosomally synthesized biologically active polypeptides containing sulfide bridges and α,β-didehydroamino acids, *Angew. Chem., Int. Ed. Engl. 30*, 1051−1068.
33. Chan, W. C., Dodd, H. M., Horn, N., Maclean, K., Lian, L. Y., Bycroft, B. W., Gasson, M. J., and Roberts, G. C. K. (1996) Structure−activity relationships in the peptide antibiotic nisin: Role of dehydroalanine 5, *Appl. Environ. Microbiol. 62*, 2966−2969.
34. Sahl, H. G., and Bierbaum, G. (1998) Lantibiotics: Biosynthesis and biological activities of uniquely modified peptides from Gram-positive bacteria, *Annu. Rev. Microbiol. 52*, 41−79.
35. Killian, J. A., Salemink, I., de Planque, M. R. R., Lindblom, G., Koeppe, R. E., and Greathouse, D. V. (1996) Induction of nonbilayer structures in diacylphosphatidylcholine model membranes by transmembrane α-helical peptides: Importance of hydrophobic mismatch and proposed role of tryptophans, *Biochemistry 35*, 1037−1045.

BI034490U